International Journal of Heat and Mass Transfer 51 (2008) 6332–6336

Contents lists available at ScienceDirect

International Journal of Heat and Mass Transfer

journal homepage: www.elsevier.com/locate/ijhmt

Technical Note

Numerical investigation of fluid flow and heat transfer characteristics by common-flow-up

J.S. Yang [a], D.W. Lee [a,b], G.M. Choi [a,c,*]

[a] RIMT, Pusan National University, Jangjeon-dong, Geumjeong-gu, Busan 609-735, Republic of Korea
[b] Department of Aerospace Engineering, Pusan National University, Jangjeon-dong, Geumjeong-gu, Busan 609-735, Republic of Korea
[c] School of Mechanical Engineering, Pusan National University, Jangjeon-dong, Geumjeong-gu, Busan 609-735, Republic of Korea

ARTICLE INFO

Article history:
Received 11 December 2006
Available online 25 August 2008

Keywords:
Vortex generator
Half-delta wing
Common-flow-up
Stanton number

ABSTRACT

Effects of the common-flow-up pair produced by vortex generators in a rectangular channel flow on fluid flow and heat transfer are numerically investigated. In order to analyze the common-flow-up pair, the pseudo-compressibility method is introduced into the Reynolds-averaged Navier–Strokes equations for a three-dimensional incompressible viscous flow. A two-layer k–ε turbulence model is applied to a three-dimensional turbulence boundary over a flat plate to predict the flow structure and heat transfer characteristics of the common-flow-up pair and to resolve the near-wall flow. Results reasonably predict the flow structure of the common-flow-up pair, such as secondary velocity vectors and turbulent kinetic energy contours. Also, in the prediction of thermal boundary layers, skin friction characteristics and heat transfer characteristics, the present results are reasonably close to the experimental results of other researchers even though some discrepancies are observed near the center of the vortex core.

1. Introduction

Longitudinal vortices are produced along their side edges by the flow separation due to the pressure difference across vortex generators. These vortices cause a rotating motion around the streamwise direction, and enhance heat transfer by mixing the fluids close to and far from the wall. Therefore, longitudinal vortices generated by vortex generators are extremely useful in many fields of engineering applications, such as the design of compact heat exchangers, cooling of hot steel plates, and automotive and aerospace industry.

Many experimental studies on the fluid flow and heat transfer related to the interaction between vortices in a turbulent boundary layer have been carried out. Eibeck and Eaton [1] conducted experiments on longitudinal vortices embedded in a turbulent boundary layer and found that the longitudinal vortices have an influence on heat transfer enhancement significantly. Metha and Bradshaw [2] reported two types of flow patterns induced by vortex generators with changing angles of attack; the flow between vortices is directed either away from the wall, common-flow-up, or toward the wall, common-flow-down. Tigglebeck et al. [3] had a thorough analysis about the influence of the geometry of the vortex generators in a rectangular channel flow. Their results showed that the delta winglet pairs present better heat transfer results. Effects of an external delta wing vortex generator on the flow and heat transfer characteristics in fan flows and uniform flows were experimentally investigated by Chen and Shu [4]. It was observed in their experimental results that the increase in the turbulent kinetic energy by the delta wing has little effect on heat transfer in the inherently vertical fan flows. Pesteei et al. [5] measured local heat transfer coefficients on a fin-tube heat exchanger with winglets using five different positions of winglet type vortex generators and found that the experimental results show a substantial increase in heat transfer with winglet type vortex generators. Pauley and Eaton [6] observed that increasing the spacing of vortex generators in the common-flow-up pair produces a dramatic increase in heat transfer enhancement since vortices with larger spacing are less able to be convected away from the wall, and reported that in the case of increasing the spacing of vortex generators the common-flow-up pair also has the same peak and minimum heat transfer coefficient as observed for the common-flow-down pair.

With experimental studies, numerical studies focusing on the interactions among vortices and boundary layers have been carried out using the vortices generated by vortex generators as models. Numerical simulations of turbulent flows in a rectangular channel with mounted vortex generators on the bottom wall were performed by Zhu et al. [7]. The flow field was computed by solving the Reynolds-averaged Navier–Stokes and energy

* Corresponding author. Address: School of Mechanical Engineering, Pusan National University, Jangjeon-dong, Geumjeong-gu, Busan 609-735, Republic of Korea. Tel.: +82 51 510 2476; fax: +82 51 512 5236.
E-mail address: choigm@pusan.ac.kr (G.M. Choi).

0017-9310/$ - see front matter © 2008 Elsevier Ltd. All rights reserved.
doi:10.1016/j.ijheatmasstransfer.2008.07.001

Nomenclature

b	height of a half-delta-wing
B	width of a rectangular channel
C	chord length of a half-delta-wing
C_f	skin friction coefficient $\left(=\tau_w/\frac{1}{2}\rho_\infty U_\infty^2\right)$
C_p	specific heat
k	turbulent kinetic energy
p	pressure
P	Pee-function
Pr	Prandtl number
Pr_t	turbulent Prandtl number
$\dot{q}$	constant heat flux
$Re_{\bar{\Delta}}$	Reynolds number based on the spanwise average enthalpy thickness
St	Stanton number $\left(=\frac{\dot{q}}{\rho_\infty C_p U_\infty \Delta T}\right)$
$\overline{St}_{sa}$	spanwise average Stanton number $\left(=\frac{2}{B}\int_0^{B/2} St dz\right)$
t	time
T	temperature
u,v,w	velocity components
U,V,W	velocity components
x, y, z	Cartesian coordinates
X, Y, Z	Cartesian coordinates
y^+	nondimensional distance from the wall in the law of the wall

Greek symbols

α	angle of attack of vortex generator
β	semi-apex angle of vortex generator
ε	dissipation rate of turbulent kinetic energy
ν	kinematic viscosity
ν_t	turbulent kinematic viscosity
ρ	density
τ	shear stress
Δ	enthalpy thickness $\left(=\int_0^\infty \frac{U(T-T_\infty)}{U_\infty(T_w-T_\infty)} dy\right)$
$\bar{\Delta}$	spanwise average enthalpy thickness $\left(=\frac{2}{B}\int_0^{B/2} \Delta dz\right)$

Subscripts

w	wall
sa	spanwise average
$*$	friction
∞	freestream

equations, and turbulence was taken into account by solving the standard k–ε model equations with the wall law. Kim and Patel [8] performed experimental and numerical studies of the interaction between the vortex and the turbulent boundary layer generated in the duct with flat plates and curvatures. Numerical and experimental investigation of flow structure and heat transfer effects of longitudinal vortices in a channel flow was reported by Biswas et al. [9]. They concluded that the winglet vortex generator shows great promise for enhancing the heat transfer rate in a plate-fin crossflow heat exchanger. Lee et al. [10] studied heat transfer characteristics and flow structure in turbulent flows through a three-dimensional turbulent boundary layer containing built-in vortex generators by using the Navier–Stokes equation and Reynolds stress transport equations. They concluded that the RSM can produce more accurate predictions to capture anisotropy of the turbulent intensities than the standard k–ε model. Chen et al. [11] studied heat transfer enhancement of a finned oval tube with staggered punched longitudinal vortex generators and concluded that winglets in staggered arrangement bring larger heat transfer enhancement than in in-line arrangement since the longitudinal vortices from the former arrangement influence a larger area and intensify the fluid motion normal to the flow direction.

As mentioned above, most of the experimental and numerical studies were to investigate the flow structure and heat transfer caused by the common-flow-down. In the case of the common-flow-up, however, only the investigation related to the flow structure was attempted restrictively.

In the present study, three-dimensional numerical analyses are performed for understanding not only the flow structure but also heat transfer generated by the common-flow-up. In order to analyze the fluid flow and heat transfer, the flow field just behind the vortex generators is modeled by the information obtained from studies on a delta wing. The flow field and heat transfer are solved by the three-dimensional Reynolds-averaged Navier–Stokes equations and energy equations for an incompressible fluid. Turbulence is modeled by a two-layer k–ε turbulent model to resolve the near-wall flow. The computational results are also compared with those of the experiment of Pauley and Eaton [6] for numerical simulation validation.

2. Numerical analysis

2.1. Governing equation

The three-dimensional Reynolds-averaged Navier–Stokes and energy equations related to the eddy viscosity concept are used to investigate the flow field and heat transfer characteristics by the common-flow-up pair. These equations can be expressed as

Continuity equation

$$\frac{\partial u_i}{\partial x_i} = 0 \tag{1}$$

Momentum equation

$$\frac{\partial u_i}{\partial t} + \frac{\partial u_i u_j}{\partial x_j} = -\frac{\partial p}{\rho \partial x_i} + \frac{\partial}{\partial x_j}\left((\nu + \nu_t)\left(\frac{\partial u_j}{\partial x_i} + \frac{\partial u_i}{\partial x_j}\right)\right) \tag{2}$$

Energy equation

$$\frac{\partial T}{\partial t} + \frac{\partial u_i T}{\partial x_i} = \frac{\partial}{\partial x_i}\left(\left(\frac{\mu}{Pr} + \frac{\mu_t}{Pr_t}\right)\frac{\partial T}{\partial x_i}\right) \tag{3}$$

The turbulent kinetic energy k and the rate of energy dissipation ε are computed from a two-layer k–ε turbulent model.

$$\frac{\partial k}{\partial t} + \frac{\partial u_i k}{\partial x_i} = \frac{\partial}{\partial x_i}\left(\left(\nu + \frac{\nu_t}{\sigma_t}\right)\frac{\partial k}{\partial x_i}\right) + G - \varepsilon \tag{4}$$

$$\frac{\partial \varepsilon}{\partial t} + \frac{\partial u_i \varepsilon}{\partial x_i} = \frac{\partial}{\partial x_i}\left(\left(\nu + \frac{\nu_t}{\sigma_\varepsilon}\right)\frac{\partial \varepsilon}{\partial x_i}\right) + \frac{\varepsilon}{k}(C_{\varepsilon 1} G - C_{\varepsilon 2}\varepsilon) \tag{5}$$

G denotes the production rate of k and is given by

$$G = -\overline{u_i u_j}\frac{\partial u_i}{\partial x_j} = \nu_t\left(\frac{\partial u_i}{\partial x_j} + \frac{\partial u_j}{\partial x_i}\right)\frac{\partial u_i}{\partial x_j} \text{ and } \nu_t = C_\mu \frac{k^2}{\varepsilon} \tag{6}$$

The coefficients are as follows:

$$C_{\varepsilon 1} = 1.44, C_{\varepsilon 2} = 1.92, C_\mu = 0.09, \sigma_k = 1.0, \sigma_\varepsilon = 1.3.$$

2.2. Numerical methodology

The turbulence model and the initial and boundary conditions are only treated because detailed descriptions of the numerical method employed in the present study, such as pseudo-compress-

ibility method and discretization and computation methods for solving the governing equations, are given in Kwak et al. [12].

2.2.1. Turbulence model

A two-layer turbulence model consisting of an inner layer and an outer layer is adopted: A one-equation model is used in the inner layer, and the standard k–ε model is used in the outer layer [8]. The one-equation model used in the inner layer needs only the solution of turbulent kinetic energy. In the inner layer, the eddy viscosity v_t is equal to $C_\mu\sqrt{k}l_\mu$, and the dissipation ratio of turbulent kinetic energy ε is equal to $k^{2/3}/l_\varepsilon$. The length scales, l_μ and l_ε, are used to give a damping effect in the near-wall according to the turbulence Reynolds number $\left(R_y = \sqrt{k}y/v\right)$.

$$l_\mu = C_l y[1 - \exp(-R_y/70)] \tag{7}$$

$$l_\varepsilon = C_l y[1 - \exp(-R_y/2C_l)] \tag{8}$$

The constant C_l is given as $\kappa C_\mu^{-3/4}$ for a smooth eddy viscosity distribution at the intersection of the inner and outer layers, where κ is the von Karman constant. This two-layer model can be used in the flow separation because the characteristic velocity near the wall is provided by turbulent kinetic energy rather than wall shear stress. Also, it does not require any boundary conditions for the computation of the dissipation ratio.

2.2.2. Initial and boundary conditions

According to Phillips and Graham [13], the velocity in the streamwise direction behind a vortex generator represents a Gaussian distribution, and the velocity in the circumferential direction appears as a Rankine vortex and the image of the Rankine vortex. Under these assumptions, the distribution of the axial velocity behind the vortex generator is given by

$$U^* = \frac{U(r)}{U_\infty} = 1 - \exp\{-\ln 2(r/r_c)^2\} \tag{9}$$

The circumferential velocity is assumed to be the form

$$V_\theta = \begin{cases} (V_\theta)_c \frac{r}{r_c} & \text{for } r\langle r_c \\ (V_\theta)_c \frac{r_c}{r} & \text{for } r\rangle r_c \end{cases} \tag{10}$$

where $(V_\theta)_c$ is the maximum circumferential velocity, r_c is the half-radius of the vortex, C is the chord length of the vortex generator, and $r_c = 0.018C$, $(V_\theta)_c = 0.501U_\infty$ and $\Gamma_c = 0.34U_\infty C$ are obtained from Polhamus [14].

When the vortices with the above velocity distribution are introduced into boundary layers, there arises a transverse velocity component parallel to the wall, and the component is not zero at the wall. Therefore, the inner leg of Johnston's triangular plot for calculating cross flow in three-dimensional boundary layers is used to represent the cross-directional velocity component [15]. Similar to the velocity in the streamwise direction, the turbulent kinetic energy and the eddy viscosity are, respectively, assumed to be a Gaussian distribution as shown below [8].

$$k(r) = k_{\max}\exp\{-\ln 2(r/r_c)^2\} \tag{11}$$

$$v_t(r) = v_{t\max}\exp\{-\ln 2(r/r_c)^2\} \tag{12}$$

And the rate of dissipation is given by

$$\varepsilon = C_\mu k^2/v_t \tag{13}$$

The maximum values of the eddy viscosity and the turbulent kinetic energy $v_{t\max} = 100v$ and $k_{\max} = 0.05U_\infty^2$ are obtained from the formula of Owen [16].

The half-delta-wing vortex generators and the installed shape of them used in the experiment of Pauley and Eaton [6] are shown in Fig. 1. The vortex generators have a chord

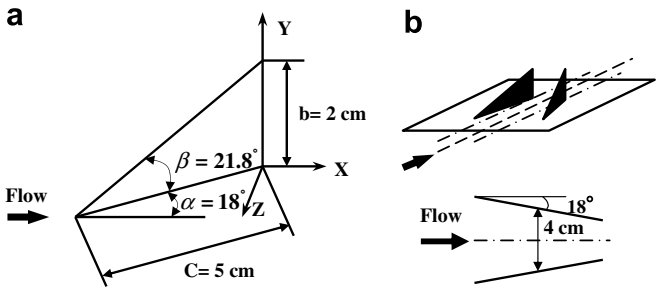

Fig. 1. Schematic of vortex generators: (a) angle of attack of a vortex generator; (b) layout of common-flow-up.

length (C) of 5 cm and semi-span (b) of 2 cm at an angle of attack (α) of $-18°$. The Reynolds number based on the chord length of the half-delta wing is 55,000. The working fluid is air and the freestream velocity is $U_\infty = 16$ m/s. The position of the vortex core is determined by referring to the α/β ratio of the delta-wing vortex generator and to a study of Lowson [17], which examined the position and form of the vortices by visualizing them. The Y and Z positions of the vortex center are 0.24C and 0.32C, respectively. Fig. 2(a) shows the physical region. Fig. 2(b) illustrates the computation domain and the boundary conditions. For the computations of the flow field, the symmetric conditions are used for the left, right, and top faces, and the Neuman conditions for the downstream region. The inlet conditions just behind the vortex generators ($X = 56.3$ cm) are given by Eqs. (9)–(13). The no-slip conditions are used in the wall, and the turbulent kinetic energy in the wall (k_w) is zero. For the temperature boundary conditions, the symmetric conditions are used for the left, right, and top faces, and the Neuman conditions for the downstream. The inlet temperature condition is constant. Also, the bottom condition is defined as follows:

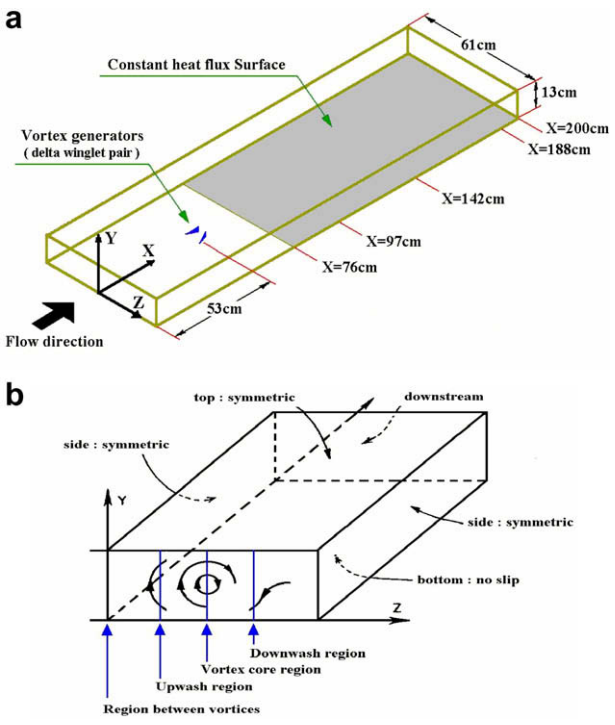

Fig. 2. Solution domain and boundary conditions: (a) physical domain; (b) computation domain and boundary conditions.

$$T_w = \frac{\dot{q}}{k} y_p + T_p \quad \text{for } y^+ \leqslant 11.63 \tag{14}$$

$$U^+ = \frac{U}{U_*} = \frac{U}{\sqrt{\frac{\tau_w}{\rho}}} \tag{15}$$

$$\frac{\rho C_p (T_w - T_p) U_*}{\dot{q}} = Pr_t (U^+ + P) \quad \text{for } y^+ \geqslant 11.63 \tag{16}$$

where y^+ and U^+ are the distance and velocity from the wall nondimensionalized by the viscosity ν, the density ρ, the friction velocity U_*, k is the thermal conductivity for air, and y_p and T_p are the distance and temperature from wall to the first grid point, respectively. The Pee-function P is correlated from pipe flow data by Jayatilleke [18] as

$$P = 9.24[(Pr/Pr_t)^{\frac{3}{4}} - 1][1 + 0.28\exp(-0.07 Pr/Pr_t)] \tag{17}$$

where the molecular and turbulent Prandtl numbers, Pr and Pr_t, are 0.7 and 0.9 for air, respectively.

For X, Y, and Z, the calculation grid point is chosen as $47 \times 80 \times 57$. In addition, the constant heat flux at the bottom wall and the temperature difference between the wall and freestream are the same as the experimental conditions. The constant heat flux and the temperature difference are taken as $\dot{q} = 817\ \mathrm{W/m^2}$ and 20 °C, respectively [6].

3. Results and discussion

The contours of secondary velocity vector among obtained results, such as velocity vector, turbulence kinetic energy, and thermal boundary layer, are show in Fig. 3 because of limited space. Fig. 3 illustrates the secondary velocity vector in the streamwise direction. The upwash flow occurs in the central plane ($Z = 0$ cm), and the downwash flow occurs outside the center plane. With the vortices developing, the magnitude of the velocity vectors decreases. The distance between the vortices does not almost change, but the lifting of the vortices from the wall increases conspicuously. As the vortices move further downstream, they are convected from the wall by the strong interaction between the vortices that move to the central plane. As a result, the vortices move up from the wall, and the shape of vortices becomes an ellipse in the vertical direction. Also the general features of turbulence kinetic energy and thermal boundary layer are well reproduced in the experimental data of Pauley and Eaton [6].

The skin friction and heat transfer coefficients in the streamwise direction are shown in Fig. 4. The values of the skin friction coefficients are larger than those of the heat transfer coefficients. In the further downstream, the positions of the maximum values

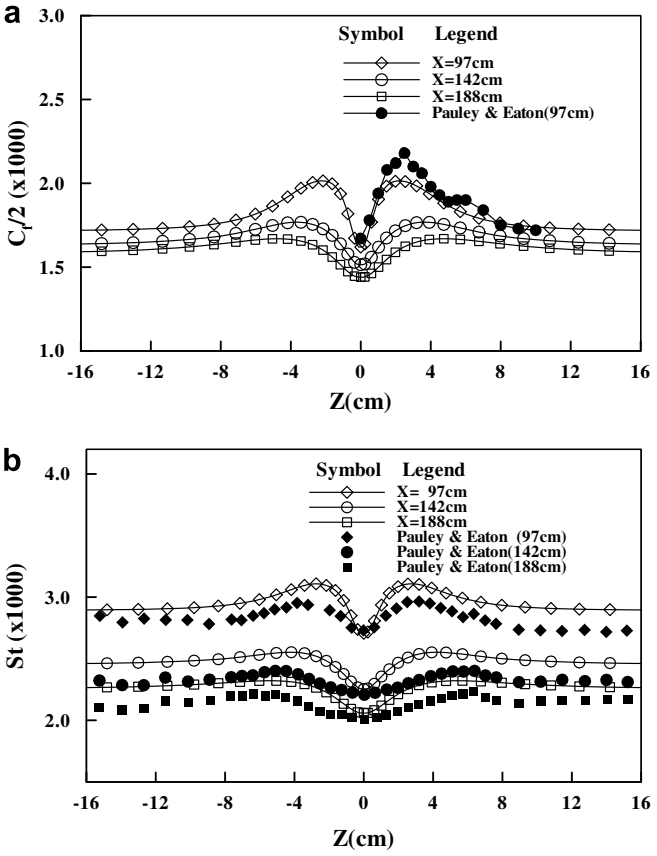

Fig. 4. Spanwise distributions of skin friction and Stanton number at $X = 97$, 142 and 188 cm: (a) skin friction; (b) Stanton number.

of the skin friction and heat transfer coefficients show little change. In the case of the skin friction, the maximum value of the skin friction coefficient obtained from the computation is predicted about 7% lower than that from the experiment at $X = 97$ cm. In the case of the Stanton number, the maximum value of the Stanton number obtained from the computation is predicted about 6%, 7%, and 5.2% higher than that from the experiment at $X = 97$ cm, 142 cm, and 188 cm, respectively. This may be caused by the isotropic assumption of the eddy viscosity model. Another reason may be inappropriate specification of the inlet boundary conditions through the vortex model. Nevertheless, the present result is assumed to well predict the experiment result.

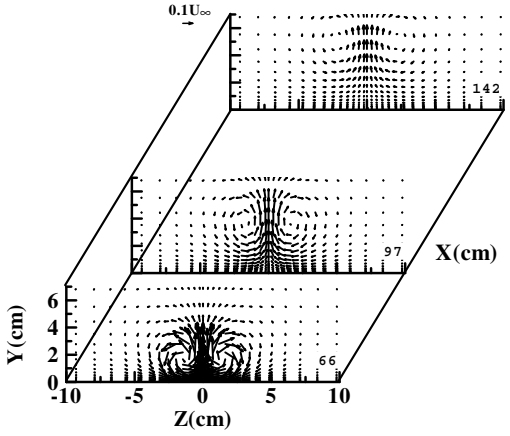

Fig. 3. Secondary velocity vectors at $X = 66$, 97, and 142 cm.

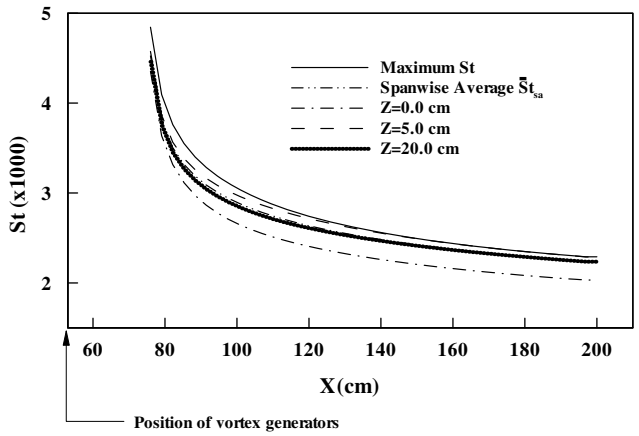

Fig. 5. Streamwise distributions of Stanton number.

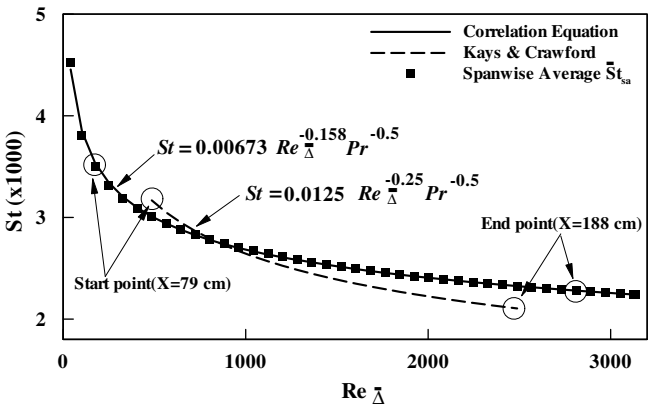

Fig. 6. Correlation of spanwise average Stanton number and Reynolds number based on the spanwise average enthalpy thickness.

The streamwise distributions of the Stanton number on different spanwise locations are shown in Fig. 5. In the range $X \leqslant 120$ cm the streamwise profiles of the Stanton number decrease rapidly. Proceeding downstream from here, they decrease gradually. In the range $X \geqslant 135$ cm the difference between the maximum and minimum values ($Z = 0$ cm) remains nearly constant. Also, there is little difference between the spanwise average Stanton number and that of $Z = 20$ cm in the whole region of the streamwise direction.

Fig. 6 shows that the $St - Re_{\bar{\Delta}}$ correlation of the present study is compared to a two-dimensional correlation based on the enthalpy thickness Reynolds number, $St = 0.0125 Re_{\bar{\Delta}}^{-0.25} Pr^{-0.5}$ [6,19]. In the present study, the correlation of the Stanton number and the Reynolds number based on the spanwise average enthalpy thickness is given by

$$St = 0.00673 Re_{\bar{\Delta}}^{-0.158} Pr^{-0.5} \tag{18}$$

The influence of the common-flow-up pair on heat transfer enhancement is maintained at the downstream location 30 times as large as the chord length of the vortex generators. In comparison with the two-dimensional correlation, the heat transfer rate caused by the common-flow-up pair is enhanced about 12.2% and 8.3% in the Stanton number over that of a plane channel at the start and end points, respectively. It is observed the decrement of heat transfer in the streamwise direction decreases gradually due to the effect of vortex generators, compared with the two-dimensional correlation. In addition, since the ratio of a frontal area of the vortex generators to a cross-sectional area of the test section is about 0.0039, the pressure drop caused by the vortex generators is not large enough to consider the pressure loss penalty.

4. Conclusion

Effects of the common-flow-up pair produced by vortex generators in a rectangular channel flow on fluid flow and heat transfer are numerically investigated.

In the case of flow field, the boundary layer is thinned in the region where the secondary flow is directed toward the wall and thickened where it is directed away from the wall. The interaction between the vortices becomes very strong while the interaction among the vortices and the boundary layers becomes very weak. As the common-flow-up pair develops, their lifting effect from the bottom wall increases more and more.

In the case of heat transfer, the distortion of thermal boundary layer is not as strong as the distortion of hydraulic boundary layer. The influence of the common-flow-up pair on heat transfer enhancement is maintained at the downstream location 30 times as large as the chord length of the vortex generators, and the correlation of the Stanton number and the Reynolds number based on the spanwise average enthalpy thickness is given by $St = 0.00673 Re_{\bar{\Delta}}^{-0.158} Pr^{-0.5}$. In comparison with the experiment of Pauley and Eaton, although some discrepancies are observed near the center of the vortex core, the overall performance of the present numerical analysis is found to be satisfactory.

References

[1] P.A. Eibeck, J.K. Eaton, Heat transfer effects of a longitudinal vortex embedded in a turbulent boundary layer, J. Heat Transf. 109 (1987) 16–24.
[2] R.D. Metha, P. Bradshaw, Longitudinal vortices imbedded in turbulent boundary layer: Part 2 Vortex pair with common flow upwards, J. Fluid Mech. 188 (1988) 529–546.
[3] S. Tigglebeck, N.K. Mitra, M. Fiebig, Comparison of wing type vortex generators for heat transfer enhancement in channel flow, J. Heat Transf. 116 (1994) 880–885.
[4] T.Y. Chen, H.T. Shu, Flow structures and heat transfer characteristics in fan flows with and without delta-wing vortex generators, Exp. Therm. Fluid Sci. 28 (2004) 273–282.
[5] S.M. Pesteei, P.M.V. Subbarao, R.S. Agarwal, Experimental study of the effect of winglet location on heat transfer enhancement and pressure drop in fin-tube heat exchangers, Appl. Therm. Eng. 25 (2005) 1684–1696.
[6] W.R. Pauley, J.K. Eaton, The fluid dynamics and heat transfer effects of streamwise vortices embedded in a turbulent boundary layer, Report No. MD-51, Department of Mechanical Engineering, Stanford University, 1988.
[7] J.X. Zhu, N.K. Mitra, M. Fiebig, Effects of longitudinal vortex generators on heat transfer and flow loss in turbulent channel flows, Int. J. Heat Mass Transf. 36 (1993) 2239–2347.
[8] W.J. Kim, V.C. Patel, Influence of streamwise curvature on longitudinal vortices imbedded in turbulent boundary layers, J. Comput. Fluid 23 (1994) 647–673.
[9] G. Biswas, N.K. Mitra, M. Fiebig, Heat transfer enhancement in fin-tube heat exchanger by winglet type vortex generators, Int. J. Heat Mass Transf. 37 (1994) 283–291.
[10] S.H. Lee, H.S. Ryou, Y.K. Choi, Heat transfer in a three-dimensional turbulent boundary layer with longitudinal vortices, Int. J. Heat Mass Transf. 42 (1999) 1521–1533.
[11] Y. Chen, M. Fiebig, N.K. Mitra, Heat transfer enhancement of finned oval tubes with staggered punched longitudinal vortex generators, Int. J. Heat Mass Transf. 43 (2000) 417–435.
[12] D.C. Kwak, S.P. Shanks, S. Chakravarthy, A three-dimensional incompressible Navier–Stokes flow solver using primitive variables, AIAA J. 24 (1986) 390–396.
[13] W.R.C. Phillips, J.A.H. Graham, Reynolds stress measurements in a turbulent trailing vortex, J. Fluid Mech. 147 (1984) 353–371.
[14] E.C. Polhamus, Prediction of vortex-lift characteristics by leading edge suction analogy, J. Aircr. 9 (1971) 193–199.
[15] J.P. Johnston, On the three-dimensional turbulent boundary layer generated by secondary flow, J. Basic Eng. (1960) 233–248.
[16] P.R. Owen, The decay of a turbulent trailing vortex, Aeronaut. Q. 21 (1969) 69–78.
[17] M.V. Lowson, Visualization measurements of vortex flows, AIAA Paper 89-0191, 1989.
[18] C.L. Jayatilleke, The influence of Prandtl number and surface roughness on the surface resistance of the laminar sublayer to momentum and heat transfer, Prog. Heat Mass Transf. 1 (1969) 193–329.
[19] W.M. Kays, M.E. Crawford, Convective Heat and Mass Transfer, McGraw-Hill, New York, 1980.